Int J Adv Manuf Technol (2012) 61:757–770
DOI 10.1007/s00170-011-3742-3

ORIGINAL ARTICLE

Studies on laser rapid manufacturing of cross-thin-walled porous structures of Inconel 625

C. P. Paul · S. K. Mishra · C. H. Premsingh · P. Bhargava · P. Tiwari · L. M. Kukreja

Received: 15 June 2011 / Accepted: 3 November 2011 / Published online: 20 November 2011
© Springer-Verlag London Limited 2011

Abstract An in-house developed continuous wave CO_2 laser-based rapid manufacturing was deployed to fabricate porous structures of Inconel-625 using a new cross-thin-wall fabrication strategy. Studies on the mechanical and metallurgical properties of these porous structures were carried out with laser energy per unit traverse length in the range of 150–300 kJ/m, powder fed per unit traverse length in the range of 16.67–36.67 g/m and transverse traverse index in the range of 0.7–1.3. The processing parametric dependence showed that the powder fed per unit traverse length was a predominating parameter in determining the porosity of the structures, followed by transverse traverse index and laser energy per unit traverse length. The compression testing of fabricated porous structures showed that the material had anisotropy up to 20% for 0.2% yield strength. It was found that the yield strength of the fabricated structures followed the power law and decreased from 423±8 MPa for 2.63±0.14% porosity to 226± 6.8 MPa for 11.57±0.52% porosity. Scanning electron microscopy showed that shape of the pores was triangular due to the cross-thin-wall fabrication strategy and the observed values of microhardness were in the range 256–370 $VHN_{0.98N}$. These studies are expected to augment our knowledge on the fabrication of porous structures with independent control on porosity and yield strength, which are important prerequisites for some of the prosthetic and engineering components in niche areas of applications.

Keywords Laser rapid manufacturing · Laser cladding · CO_2 laser · Porous structure · Inconel-625 · Cross thin-wall fabrication strategy

1 Introduction

Porous materials are quite common in nature. Bone, a naturally engineered porous structure, allows birds to fly due to its lower density while animals can crawl on the ground due to relatively dense bones. Until recently, porosity was considered one of the harmful defects that impede efficiency or functional properties of the mechanical components, limiting its applications to non-load-bearing applications, such as filtration, flow control, thermal and/or acoustic management [1]. However, if porous structures with adequate mechanical strength can be produced, they can find direct applications as light-weight structural, functional materials, transportation materials, etc. [2, 3]. This encouraged research towards the development of porous structures with tailored mechanical properties. Conventionally, furnace sintering technique, space holder technique, replication technique and combustion synthesis technique are used for fabrication of porous structures with non-homogenous pores, while orderly oriented wire mesh technique, ferromagnetic fiber arrays technique and vapor deposition technique are used for

C. P. Paul (✉) · S. K. Mishra · C. H. Premsingh · P. Bhargava · L. M. Kukreja
Laser Materials Processing Division,
Raja Ramanna Centre for Advanced Technology,
Indore 452 013, India
e-mail: paulcp@rrcat.gov.in
URL: http://www.rrcat.gov.in/technology/laser/lmpd/index.html

P. Tiwari
Indus Synchrotrons Utilization Division,
Raja Ramanna Centre for Advanced Technology,
Indore 452 013, India

fabrication of porous structures with homogenous pores [4]. But all these techniques have limitations in the fabrication of porous structures with engineered mechanical properties due to their inability to precisely control a number of parameters: pore size, shape, volume fraction, pore-distribution, contaminations and their phases, etc. Moreover, they cannot be used to generate functionally designed porous structures with graded porosity. Such structures can be potentially fabricated using layered manufacturing techniques, like three-dimensional printing [5], laser rapid manufacturing (LRM) [6].

LRM is one of the fastest emerging rapid-manufacturing technologies used to fabricate next-generation "feature based designed and manufacturing" products and to repair existing prime components at lower cost with improved functionality. The advantages of this methodology are established, and this is being abundantly used by different researchers for the fabrication of complex engineering components particularly of scarce materials. Researchers from the Sandia National Laboratory (USA) have focused on creating complex metal parts [7]. The National Research Council of Canada has developed the technology for the manufacturing of structural components for advanced robotic and mechatronic system [8]. Researchers at the University of Waterloo, Canada, have developed a method to produce WC-reinforced hard surfaces on low carbon steel [9]. The underlying technologies for the laying critical surfaces on prime components have been developed at the University of Liverpool, UK [10]. Recently, control of melt pool temperature and deposition height during LRM process has been developed at the University of Michigan, USA [11]. LRM has been deployed for the laser deposition of high-performance materials at the University of Manchester, UK, and Fraunhofer Institute, Germany [12, 13]. Imran et al. [14] reported an LRM-based novel approach to replace a conventional steel die by a bimetallic die made of Moldmax copper alloy coated with a protective layer of steel on the cavity surface for high-pressure die casting of aluminum alloys.

LRM has also been one of the major research mandates at our laboratory for about the past 8 years. In our earlier efforts, the components of Colmonoy-6 (a Ni-based hardfacing alloy) were fabricated using LRM, and their mechanical and metallurgical properties were found to be comparable to that of conventionally processed components [15]. Another Ni-based alloy, Inconel-625, was used for the LRM of various structures, and their mechanical and metallurgical properties were investigated [16]. Fatigue and fracture characteristics of laser rapid manufactured structures of Inconel-625 were also studied [17]. All these works were focused on bulk behavior of fully dense laser rapid manufactured structures. Lately, we have undertaken the LRM of porous structure at our laboratory. This initiative envisages the fabrication of functional metal parts or high-performance surfaces by LRM for prosthetic and engineering applications using different metals, including stainless steel, nickel-based alloys, titanium alloys, in a controlled environment. Although this methodology offers numerous advantages, there are also a variety of problems: material vaporization, lack of fusion, part porosity, part shrinkage, cracking, delaminating layer, etc. [18, 19].

Recently, some of the limitations of laser based rapid manufacturing techniques like part porosity, lack of fusion, were exploited in a controlled way to its strength and were used for the fabrication of viable porous structures. Most of these studies are focused on laser-assisted sintering technique. Gu and Shen [20] studied the processing conditions and microstructural features of porous SS316L by directed metal laser sintering. Li et al. [21, 22] focused on the densification behavior of metal powders and its effects on the fabrication of graded porous structures during selective laser sintering. Krishna et al. [23] employed LRM for the fabrication of porous structures of Ti with broad range of compressive yield strength between 21 and 463 MPa and a low Young's modulus between 1.7 and 28 GPa. Recently, a diode laser in continuous mode and a CO_2 laser in pulsed mode were used to produce multilayer porous structures. A comparison between them with respect to their internal geometry, pore size, and part density using a range of techniques including micro-tomography was reported by Ahsan et al. [5]. However, to the best of our knowledge, the fabrication of porous structures employing cross-thin-wall fabrication method has not been reported in the literature.

In the present study, LRM was employed for the fabrication of structures of Inconel-625 with different degree of porosity using a new cross-thin-wall fabrication strategy. The effect of processing parameters—such as laser energy per unit traverse length, powder feed per unit traverse length, transverse traverse index, number of layers—was studied to understand the mechanical and metallurgical properties of the ensuing structures. Box–Behnken design of response surface methodology was used to model the porosity in terms of processing parameters and their influence on the resultant porosity. Further, the fabricated porous structures were also characterized using various mechanical tests (e.g., compression testing, microhardness measurements) and various microscopic techniques (e.g., optical microscopy, scanning electron microscopy, energy-dispersive spectroscopy). The results of these tests and studies are presented and discussed in this report.

2 Experimental details

2.1 Details of material

Inconel-625 is one of the nickel–chromium-based alloys widely used for various naval, aerospace and nuclear applications. It has an outstanding fatigue and thermal-fatigue strength, good oxidation and corrosion resistance, excellent resistance to stress corrosion cracking and pitting resistance at elevated temperature, and excellent characteristics for welding and brazing [24]. It derives its strength from the stiffening effect of molybdenum and niobium on its nickel–chromium matrix; thus, precipitation–hardening treatments are not required [25]. Thus, Inconel-625 is an alloy with many ongoing and potential applications in various engineering industries. We have demonstrated earlier that laser rapid manufactured Inconel-625 components, having mixed microstructures of cellular and dendrites, had higher yield strength than and nearly identical percentage elongation as that of their wrought counterparts [16]. Dinda et al. [26] demonstrated that directionally solidified components of Inconel-625 could be prepared or repaired by LRM with an appropriate processing strategy. Considering their widespread applications and oxidation-resistant property, the fabrication of porous structures of Inconel-625 was taken up in the present study. The chemical composition of the alloy under investigation is presented in Table 1.

2.2 LRM strategy

LRM, being a layer-by-layer additive manufacturing technique, has a unique feature to deposit the material selectively at the desired points. The locus of these desired points is called “LRM strategy”. Various LRM strategies can be used to fabricate the porous structures with different bulk porosity or the porous materials with same porosity and different mechanical properties. There are a number of LRM strategies, which include cross-thin-wall fabrication method, recursive ball deposition method. In cross-thin-wall fabrication, the porous material is fabricated by depositing the material in mutually orthogonal directions among the successive layers, while in recursive ball deposition method, the small balls are fabricated one upon another to fabricate the porous material by using laser in pulsed mode [5]. Figure 1 shows the schematic representation of these LRM strategies. In our earlier work, the recursive ball deposition method was employed to fabricate the porous material of stainless steel AISI 316 L, and a porosity of around 28% was achieved, but these materials did not have adequate mechanical strength due to the oxidized non-uniform joints among successive balls [27]. This work is focused on cross-thin-wall fabrication method.

Table 1 Nominal composition (wt.%) of the powder used for laser cladding

Material	C	Cr	Ni	Si	Mo	Fe	Ti	Al
Inconel-625	0.1	22.5	62.2	0.5	9.2	4.7	0.36	0.4

2.3 Experimental setup

This study was carried out using an in-house integrated LRM system. It consisted of an indigenously developed 3.5-kW CW CO_2 laser system [28], a co-axial powder-feeding nozzle with a volumetric controlled powder feeder [29] and a five-axis CNC laser workstation. Figure 2a and b presents the schematic arrangement and photograph of the experimental setup. The CO_2 laser beam was transferred to a five-axis CNC laser workstation by steering the beam with the water-cooled gold coated plane copper mirrors. A concave mirror (radius of curvature=600 mm) at an inclination angle of about 22º was used to focus laser beam at the laser workstation, and a defocused beam of diameter about 1.2 mm was delivered at the fabrication point for LRM. Argon gas was used as shielding and carrier gas. The size of the powder particles used in the study was in the range between 45 and 106 μm. The distribution of the particle size in the Inconel-625 powder under investigation was measured by standard sieving and weighing technique. The measured values were 94.5%, 12.7% and 1.5% for <90, <75 and <63 μm, respectively. LRM of the Inconel-625 tracks was carried on austenitic stainless steel AISI 316 L substrates of diameter 75 and 12 mm thick. Prior to the experiments, the substrates were sand-blasted to roughen the machined surface so as to increase the laser absorption [18].

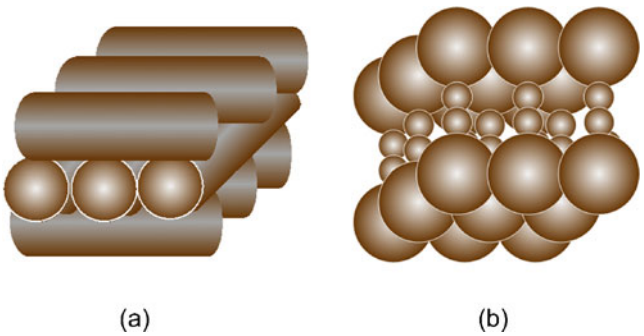

Fig. 1 LRM strategies: **a** cross-thin-wall fabrication and **b** recursive ball deposition

2.4 Process parameters

In order to optimize the process parameters, a number of tracks were deposited at different process parameters. The uniform tracks without porosity were selected by visual examination. To investigate the porosity and uniformity of the tracks, they were sectioned normal to traverse direction using standard metallographic techniques. They were subsequently studied under optical microscopy. The effect of processing parameters and their selection criteria are presented in Section 3.1. Table 2 summarizes the process parameters used for the above experiments. The processing parameters laser power, scan speed and powder feed rate have major role in the formation of the single track for particular LRM system configuration [18]. However, we find that the effect of these three parameters can be accounted with the following two parameters:

$$\text{Laser energy per unit traverse length } (E_l) = \frac{\text{Laser Power}(P_L)}{\text{Scan Speed}(V_s)} \quad (1)$$

$$\text{Powder fed per unit traverse length } (m_{p/l}) = \frac{\text{Powder feed rate}(m_p)}{\text{Scan Speed}(V_s)} \quad (2)$$

Pore and void formation during LRM on a plane surface can be divided into three categories: inter-run porosity, porosity due to interlayer lack of fusion and intralayer porosity [30]. Inter-run porosity is caused between two neighboring tracks due to lack fusion in deposited material near the base of the deposited tracks. Interlayer lack of fusion porosity is caused by incomplete bonding between adjacent layers. Intralayer porosity is often the spherical areas of porosity within a layer—its cause is not always clear but is thought to be related to gas dissolved or entrapped within the melt. Apart from these, the porosity can also be because of misplaced tracks, an oxide layer preventing or hindering fusion, and initial porosity in the particles, which might get modified during the LRM process [17]. The formation of such porosity is considered a limitation of the LRM process. In the present study, this limitation is exploited to shape porous materials. This study is focused on fabricating porous structures at various transverse traverse indices with different combination of "laser energy per unit traverse length" and "powder fed per unit traverse length". The transverse traverse index is ratio of the distance between two subsequent tracks to track width. Mathematically,

$$\text{Transverse traverse index } (i) = \frac{x}{W} \quad (3)$$

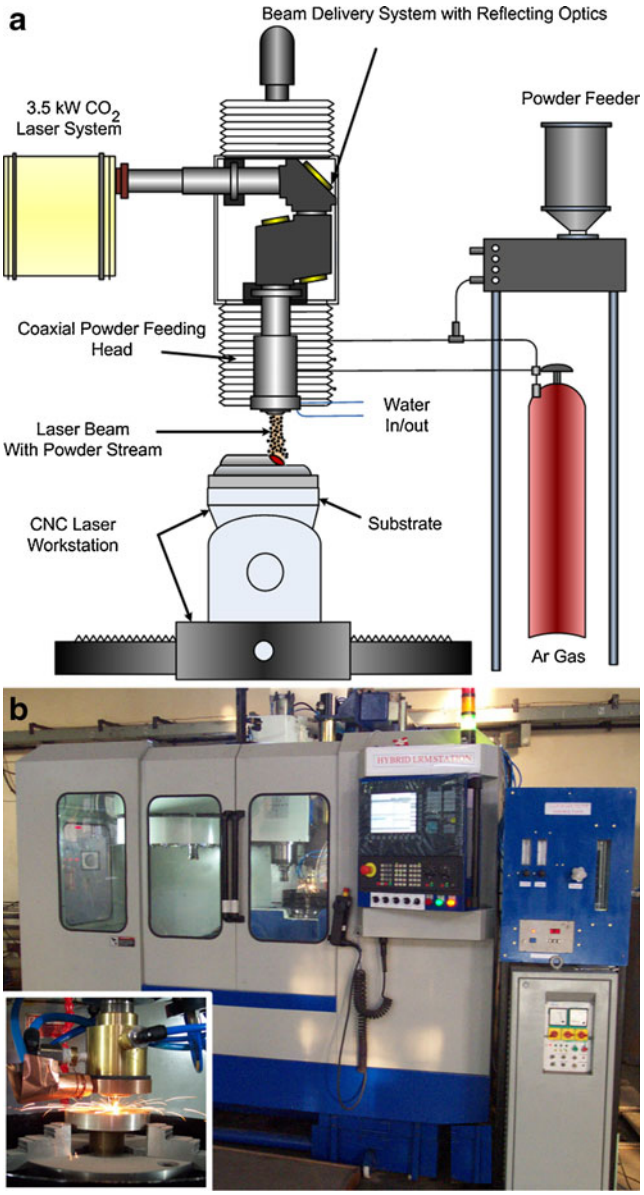

Fig. 2 **a** Schematic arrangement of laser rapid manufacturing setup. **b** Photograph of laser rapid manufacturing setup with co-axial processing head in *inset*

Table 2 Range of processing parameters used in experiments

Parameter	Unit	Values
Laser power (P_L)	kW	0.75–1.5
Powder feed rate (V_s)	g/min	5–11
Scan speed (m_p)	m/min	0.3

2.5 Design of experiments

The response surface method was employed for developing empirical model for predicting yield parameter "percentage porosity" under a set of controlled experimental factors. Basically, this optimization process involved three major steps: performing the statistically designed experiments, estimating the coefficients in a mathematical model, and predicting the response and examining the adequacy of the model [31, 32]. The significant variables, laser energy per unit traverse length, powder fed per unit traverse length and transverse traverse index, were chosen as the critical variables designated as X_1, X_2 and X_3, respectively. The values of X_1 and X_2 were selected within the obtained processing window, as described in Section 3.1. Generally, fully dense structures laser rapid manufactured using transverse traverse index (X_3) closer to 0.6. Therefore, we have chosen variable X_3 in the range of 0.7–1.3. The low, middle, and high levels of each variable were designated as −1, 0 and +1, respectively (see Table 3). The Box–Behnken design was selected for carrying out experiments, because relatively few experimental combinations of the variables were adequate to estimate potentially complex response functions. A total of 15 experiments were necessary to estimate the seven coefficients of the model using multiple linear regression analysis. Various combinations of LRM parameters used in the present study are summarized in second, third and fourth columns of Table 4.

The significance of relationships between the process variables and their effect was established by analysis of variance (ANOVA). In a system involving three significant independent variables, X_1, X_2 and X_3, the mathematical relationship of the response in terms of independent parameters and interacting parameters can be given by the equation [33]:

$$Y = C_0 + C_1X_1 + C_2X_2 + C_3X_3 + C_{12}X_1X_2 + C_{13}X_1X_3 + C_{23}X_2X_3 \quad (4)$$

where Y is the predicted yield, C_0 is constant, C_1, C_2 and C_3 are the linear coefficients, C_{12}, C_{13} and C_{23} are the cross-product coefficients. A multiple regression analysis was done to obtain the coefficients and the equation could be used to predict the response.

Table 3 Processing parameters selected for three level experiments

Parameters	−1	0	+1
Laser energy per unit traverse length (kJ/m), X_1	150	220	300
Powder fed per unit traverse length (g/m), X_2	16.67	26.67	36.67
Transverse traverse index, X_3	0.7	1.0	1.3

Table 4 Experimental parameters as per Box–Behnken approach and obtained porosities

Sample ID	E_l (kJ/m)	$m_{p/l}$ (g/m)	i	Porosity* (%)	σ_{std}*
200901501	300	16.67	1.0	2.634	0.137
200901502	150	16.67	1.0	5.191	0.245
200901503	225	16.67	1.3	6.210	0.205
200901504	225	16.67	0.7	3.208	0.278
200901505	225	26.67	1.0	4.308	0.080
200901506	150	26.67	1.3	1.750	0.406
200901507	150	26.67	0.7	7.683	0.377
200901508	225	26.67	1.0	4.011	0.148
200901509	300	26.67	1.3	9.390	0.415
200901510	300	26.67	0.7	3.674	0.072
200901511	225	36.67	0.7	9.632	1.199
200901512	150	36.67	1.0	9.800	0.342
200901513	300	36.67	1.0	11.380	0.706
200901514	225	36.67	1.3	11.570	0.521
200901515	225	26.67	1.0	4.180	0.103

2.6 Material characterization and testing

The fabricated porous materials were subjected to various mechanical and metallurgical tests to evaluate their properties. First, the samples were machined and ground to a regular size of 5 mm^2 cross-section and 10 mm length within the measurement accuracy of ±0.05 mm. The actual sizes and weight of these prepared samples were measured and porosity was calculated using the following relations:

$$\%\ \text{Porosity} = 1 - \frac{\text{Measured Weight of Sample}}{\text{Measured Volume of Sample} \times \text{Solid Density}} \quad (5)$$

The porous samples were cut, epoxy potted, ground and polished for microscopic studies. The microscopic studies were carried out using optical microscopes (Nissho Optical, Model: TZ-240; Olympus, Model: PME3) and scanning electron microscope (Philips, Model XL30). Energy dispersive X-ray spectrometer (EDS) attached with SEM was used to confirm the chemical composition on the transverse section of laser rapid manufactured porous structures.

These samples were subjected to compression testing to evaluate their mechanical properties as per the American standard test method of compression testing of metallic materials at room temperature, ASTM standards [34]. These tests were conducted on a BiSS, India-made computerized servo-hydraulic 150 kN universal testing

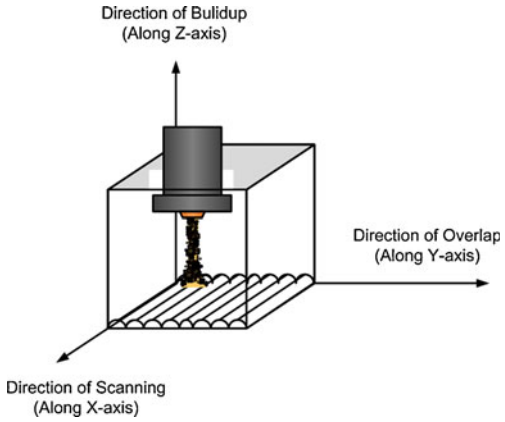

Fig. 3 Nomenclature describing the various directions during LRM

machine. Figure 3 presents the nomenclature used in the sample to indicate the various directions, associated with LRM of these samples. The relation between yield strength and porosity was evaluated.

Vickers microhardness measurement was performed on the cross-section of the laser rapid manufactured porous structures using Leitz Mini load-2 microhardness tester with a load of 100 g, as per ASTM standards [35].

3 Results and discussion

3.1 Effect of processing parameters

Since LRM involves a number of processing parameters, it is desirable to optimize the manufacturing parameters in a mutually coordinated manner to accomplish the fabrication of the components/structures. For this reason, the shape and dimensions of the transverse cross-section of the single tracks and the deposition rate with the variation of the processing parameters continue to be one of the areas of contemporary research in LRM. There are several analytical, numerical and empirical models developed to predict the track geometry [36–39]. Analytical and numerical simulations have limitations due to simplifications/assumptions during modeling, while empirical relations are valid for the particular system configurations. Therefore, a quantitative understanding of the relationship between independent process parameters and the formation of single tracks of Inconel-625 was undertaken in the present study.

The parameters "laser energy per unit traverse length" and "powder fed per unit traverse length" govern the laser energy and the material available for the single track deposition, respectively. At extremely high laser energy per unit traverse length and lower powder fed per unit traverse length, there may be vaporization of the feed material. As a result, there may be very thin or no track formation. On the contrary, at extremely low laser energy per unit traverse length and higher powder fed per unit traverse length, the feed material may not fuse and form a discontinuous track. Hence, there is a processing window, where there is balance of both the parameters, resulting in fused continuous tracks. The optimum process window is found to be 120–360 kJ/m for laser energy per unit traverse length and 10–40 g/m for powder fed per unit traverse length. Figure 4 presents the effect of the laser energy per unit traverse length and powder fed per unit traverse length on single track width and height. It may be noted that track width and height are primarily governed by the parameter "powder fed per unit traverse length", and they increase as this parameter is increased. The variation of 100% in "laser energy per unit traverse length" is found to result the maximum variation of only 20% in width and height of the single track. Thus, the increase in "laser energy per unit traverse length" has little influence on the track geometry. This is in agreement with the results obtained by Pinkerton et al. [40].

Multilayer deposition on a single track is required to shape the single wall of the three-dimensional porous structure fabricated using LRM. The effect of processing parameters, i.e., "laser energy per unit traverse length" and

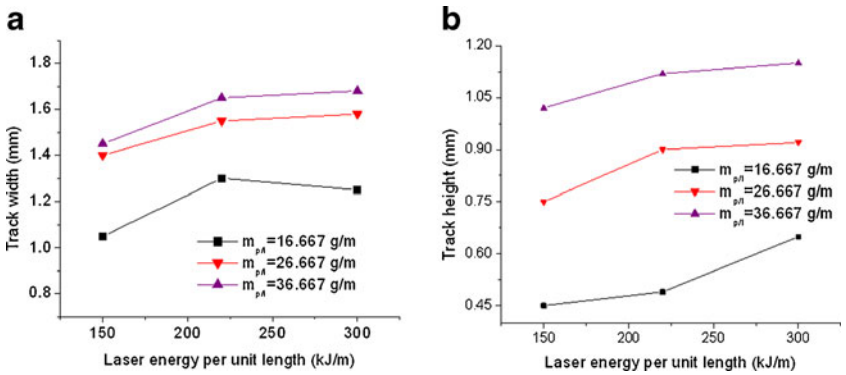

Fig. 4 Effect of laser energy per unit traverse length and powder fed per unit traverse length on single track: **a** width and **b** height

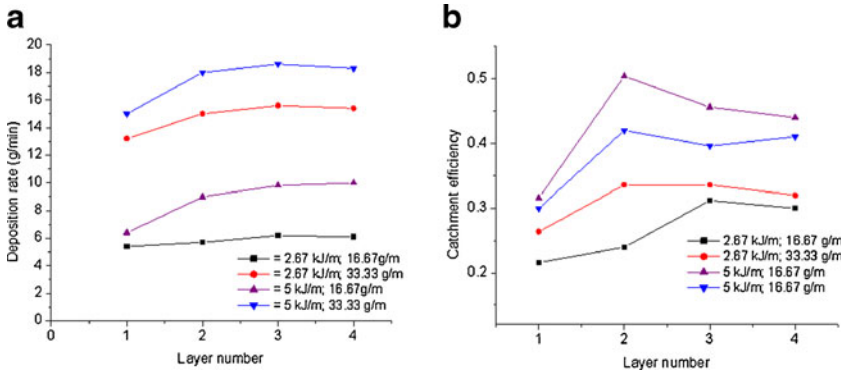

Fig. 5 **a** Material deposited per unit length and **b** catchment efficiency as a function of number of layers at various "laser energy per unit traverse length" and "powder fed per unit traverse length"

"powder fed per unit traverse length" as a function of number of layers of a single wall were investigated. Figure 5a and b shows the material deposited per unit length and catchment efficiency, respectively, in different number of layers at various "laser energy per unit traverse length" and "powder fed per unit traverse length". Figure 5a shows that the material deposited per unit traverse length increased from first layer to second layer and in subsequent layer, it tended to saturate. Figure 5b shows that the catchment efficiency enhances from the first layer to the second layer, which could be attributed to the enhancement of surface area of melt pool when one goes from the flat surface of the substrate to convex surface of the first layer of track. The improvement in the catchment efficiency results in the increased material deposition per unit traverse length in the second layer, as shown in Fig. 5a. The variation of catchment efficiency at higher number of layers shows enhanced randomness as observed in Fig. 5b. This might be because the catchment efficiency is based on very complex processes such as ricochet effects, adhesion and recoil of the incoming preheated powders at the molten pool and surrounding solid surface of the substrate. Consequently, a large scatter in experimental data is obtained, as shown in Fig. 5b.

Figure 5a also shows that as the laser energy per unit traverse length was increased, there was increase in the track width and track height, leading to higher material deposition per unit traverse length. Similarly, with increased powder fed per unit traverse length, the mass deposited per unit traverse length also observed to increase as shown in Fig. 5a. In contrast with this, the catchment efficiency decreased with the increase in powder fed per unit traverse length and increased with increase in the laser energy per unit traverse length. However, the increase in the catchment efficiency with increase in the laser energy per unit traverse length was much higher at lower powder fed per unit traverse length, as compared to that at higher powder fed per unit traverse length, as shown in Fig. 5b. These results are understandable based on the consideration of amount of powder melts by the interacting laser beam and the fraction of the mass of the powder that get attached to the layers in a track. Based on the above observations, a number of porous structures were fabricated as per "design of experiment". Figure 6 presents a typical laser rapid manufactured porous structure.

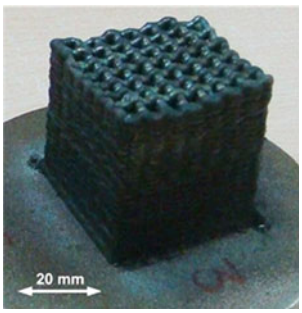

Fig. 6 A typical laser rapid manufactured porous structure

3.2 Porosity

Table 4 summarizes the porosity achieved at various combinations of process parameters. The values of process parameters and obtained porosity were subjected to ANOVA to identify the predominant processing parameters and their effects. The results are presented in Table 5. The standard F-test parameter showed the significance of each parameter in the process and p value indicated the probability of its occurring, if the null hypothesis was true [33]. The data in Table 5 indicate that the powder fed per unit traverse length was very important independent process parameter and governed the porosity. Next to powder fed per unit traverse length, transverse traverse index contributed to the porosity, as an independent parameter, while laser energy per unit traverse length had a little effect on the porosity as independent parameter. As the powder fed per unit traverse length and transverse traverse index were increased, the porosity increased. As per ANOVA, laser

Table 5 Analysis of variance (ANOVA) of processing parameters and porosities

Parameters	Degree of freedom	Sum of squares	Mean square	F ratio	p Value
E_l	2	0.921	0.460	0.761	0.0482
$m_{p/l}$	2	187.944	93.972	155.372	2.24×10^{-11}
i	2	6.812	3.406	5.631	0.013
$E_l \times m_{p/l}$	3	14.163	4.721	7.806	1.72×10^{-3}
$E_l \times i$	2	63.974	31.987	52.887	5.028×10^{-8}
$m_{p/l} \times i$	1	1.102	1.103	1.823	0.0195
Error	17	10.282	0.605		
Total	29	285.198	136.254		

energy per unit traverse length had the least influence on resultant porosity; it is because laser energy per unit traverse length does not show a consistent trend for experimental observed porosity. At the lower powder fed per unit transverse length, porosity decreased with the increase in laser energy per unit transverse length. This may be because of flattening of the track geometry, leading to higher packing factor (=filled volume/total volume) in the track geometry cross-section. On the contrary, at higher powder fed per unit traverse length, the porosity increased with increase in laser energy per unit traverse length; this may be because of the increased track geometry aspect ratio, leading to lower packing factor in the track geometry cross-section. However, it reconfirmed that there was sufficient laser energy per unit traverse length was available to melt and deposit the fed powder for LRM in the range under investigation. The predominance of powder fed per unit traverse length was largely due to the variation in the aspect ratio of the tracks, resulting in change in packing factor of the track cross-section and track geometry shape. For the same track width, the increase in the powder fed per unit traverse length resulted in higher track height and reduced aspect ratio. This shifted the shape of the track towards the circular shape from the segment of a circle and increased the porosity.

As per ANOVA, the combined effect of laser energy per unit traverse length and transverse traverse index had the maximum contribution to the porosity. This is because, at the higher laser energy per unit traverse length and lower transverse traverse index, there was higher material deposition for respective rectangular cross-sectional area and as a result, the porosity was lower. Similarly, at the lower laser energy per unit traverse length and lower transverse traverse index, there was higher material deposition with smaller cross-sectional area and the porosity remained lower. On the other hand, at the lower laser energy per unit traverse length and higher transverse traverse index, there was lesser material deposition for the same rectangular cross-sectional area and subsequently, the porosity was higher, while at the higher laser energy per unit traverse length and higher transverse traverse index, there was lesser material deposition with bigger cross-sectional area and subsequently, the porosity was the highest.

For the range of the parameter under investigation, the surface response of the porosity as a function of laser energy per unit traverse length (E_l), powder fed per unit traverse length ($m_{p/l}$) and transverse traverse index (i) was computed and presented in the following equation:

$$\begin{aligned}\text{Porosity}(\%) = {} & 14.2843 - 0.12105\, E_l + 0.2432\, m_{p/l} \\ & - 6.9277\, i + 1.379 \times 10^{-3}\, E_l\, m_{p/l} \\ & + 0.0811\, E_l\, i - 0.2196\, m_{p/l}\, i \end{aligned} \quad (6)$$

Figure 7 shows a representative surface response of the above experiments, indicating the effect of transverse traverse index and powder fed per unit traverse length on porosity as per the equation given above for laser energy per unit traverse length at 225 kJ/m.

3.3 Microscopic examination

The microscopic examination of the porous samples was carried out using optical microscope and scanning electron microscopy. Figure 8 shows optical micrographs of repre-

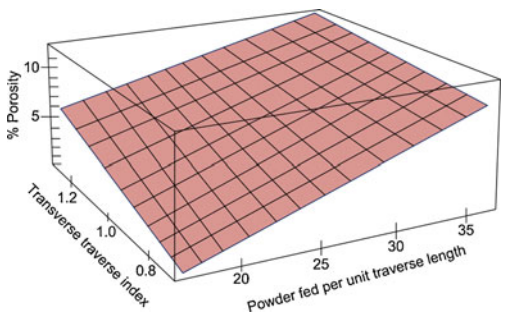

Fig. 7 Effect of transverse traverse index and powder fed per unit traverse length on porosity as per the equation given above for laser energy per unit traverse length at 225 kJ/m

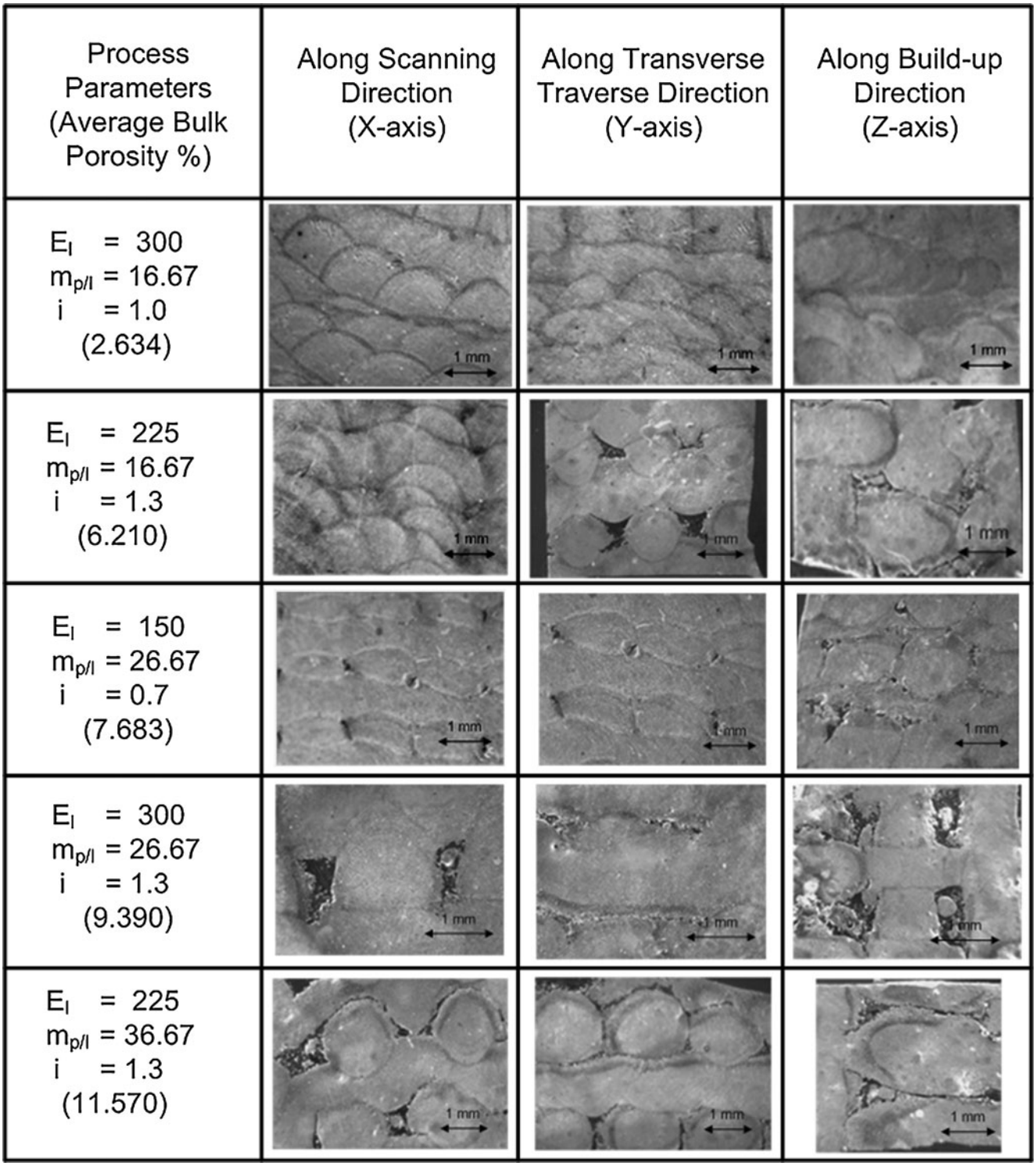

Fig. 8 Optical micrographs of representative porosities on cross-sections along different directions of laser rapid manufactured structure of Inconel-625

sentative porosities on cross-sections along different directions, i.e., plane normal to scanning direction (*X*-axis), plane normal to transverse traverse direction (*Y*-axis) and plane normal to the build-up direction (*Z*-axis) of the laser rapid manufactured structure of Inconel-625 under different deposition conditions. As shown in Fig. 8, the resultant

laser rapid manufactured specimens have pores, arranged in the form of regular arrays. The location of these pores is at the junctions of adjacent tracks and adjoining layers, specifically at the track overlap region. The size of the pores is not uniform at various locations within the same sample, and it can be seen that the average bulk porosity increases due to increase in the pore size. The shape and size of the pores are different on three different planes, indicating that the resultant porous structures will have anisotropy in mechanical properties. The shape and size of the pores on the planes normal to *X*- and *Y*-axes are nearly the same. Therefore, it is expected that the mechanical properties along these two axes are largely similar. It may also be noted that lower porosity is achieved with larger track aspect ratio (track width/track height), while higher porosity is achieved when track aspect ratio is close to unity. This is attributed to the fact that with increase in the aspect ratio, the cross-section of the clad track is a segment of circle, and it is almost a circle at aspect ratio close to unity. The observed microstructure was associated with mostly columnar dendrites that grew epitaxially from the substrate/preceding layer with the direction of columnar dendrites same as the direction of laser scanning. Similar trends were also observed by Dinda et al. [26].

Figure 9 presents typical inter-track joints at various processing parameters. As described earlier, there were porosities at the inter-track region. The shape of these pores was triangular due to the adopted LRM strategy, and they were formed due to the inherent rapid solidification of the metal track. The size of the pore was the function of the location within the track and it also depended on LRM processing parameters. The trapped unfused powder particles were also observed in some of the pores. It was noted that the microstructure formed were different at the various neighboring regions of the inter-track joints due to the different cooling rates. The fine dendrites were observed at the outer surface of tracks, the direction of growth was radially out towards the pore with the orientation preferentially from the base of the track. A typical result of EDS analysis of fabricated porous structure is presented in Fig. 10 and Table 6. It reconfirms that there was no measurable change in the composition of the Inconel-625 during LRM.

3.4 Compressive strength testing

Figure 11 presents a typical engineering stress–strain curve obtained during compressive strength testing of the laser rapid manufactured porous materials. The curve indicated that there was sharp increase in stress with small compression in the beginning up to point A. This was region of elastic and small plastic deformation. Therefore, this slope is not generally used to determine the Young's modulus of the porous materials. The associated plastic deformation in this region is responsible for mechanical damping. After the initial increase in stress, there was then a change to a regime of plastic deformation, where small increase in stress resulted in larger compression up to point B. The measured value of porosity at this point was less than 10% of the initial value. After an extended plateau regime, the curve finally changed to densification, when the porosity was negligible with neighboring tracks completely coalescing with each other. The measured value of porosity was negligible at this point.

The micrograph placed as inset between O and A shows the cross-section of the laser rapid manufactured porous material at the beginning of compression test. In this micrograph, the pores are clearly visible and cross-sectional shape of the tracks is nearly circular. The micrograph placed between A and B shows the cross-section of the laser rapid manufactured porous material after compression near the point B. In this micrograph, the pores and tracks are of elongated shape due to compression. The pores are compressed and almost filled with material flow. This flow of the material gives rise to plateau regime in the stress strain curve. The slope and length of the curve in plateau region depends on the rate of densification of the material, which is primarily governed by the interaction

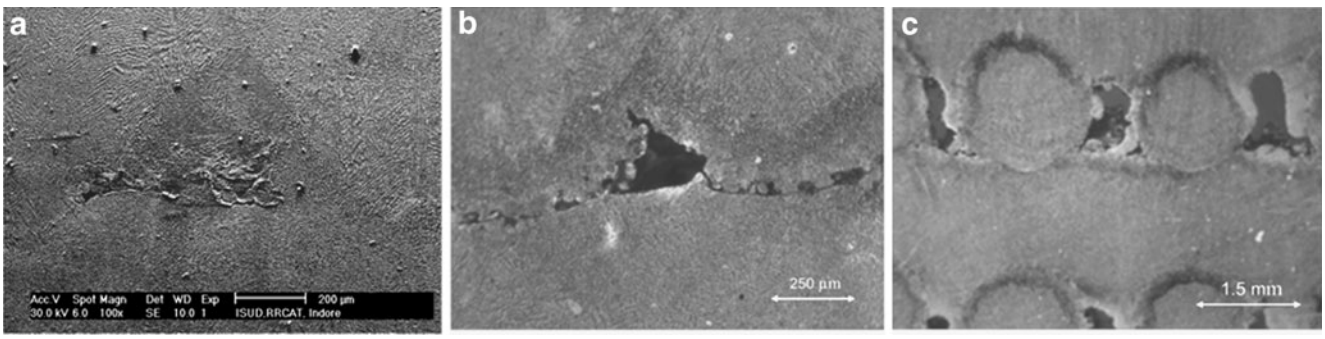

Fig. 9 Typical inter-track joints at various processing parameters

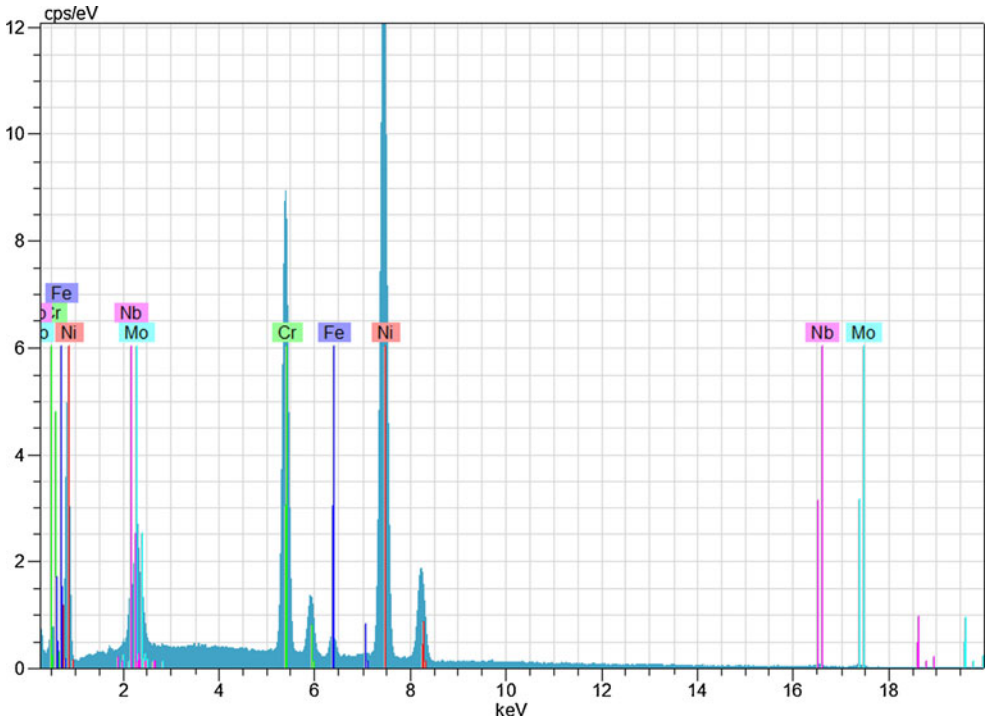

Fig. 10 Result of Energy dispersive X-ray spectroscopy

between the pores and wall within the porous material [41]. The micrograph near point C shows the cross-section of totally compressed porous material. The neighboring tracks are compressed together and completely deformed shape of the pore is clearly visible.

Figure 12 presents the 0.2% yield strength as a function of the porosity. The curve fitting of experimental values with error (between experimental and curve-fit value) less than 5% confirms the following empirical relation [42]:

$$\mathrm{YP}_{\mathrm{porous}} = \mathrm{YP}_{\mathrm{Solid}}\left(1 - \frac{\rho_{\mathrm{porous}}}{\rho_{\mathrm{solid}}}\right)^{k} \tag{7}$$

where $\mathrm{YP}_{\mathrm{porous}}$ and $\mathrm{YP}_{\mathrm{solid}}$ are the 0.2% yield strength of porous and solid material, respectively, while ρ_{porous} and ρ_{solid} are their corresponding density. k is the empirical constant that depends on material and fabrication method.

Table 6 Typical result of energy dispersive X-ray spectroscopy of fabricated porous structure

Element	Average chemical composition (wt.%)	Average observed composition (wt.%)	Error (%)
Ni	62.2	62.09	1.6
Cr	22.5	21.71	0.6
Mo	9.2	8.52	0.5
Fe	4.7	1.66	0.1
Nb+Ta	3.6	3.93	0.3

For the method under investigation, the value of k is 0.17. It may be noted that the yield strength decreases faster with the increase in the porosity, because the mechanical properties are highly sensitive to microstructural parameters: pore size, shape, orientation, distribution, etc. These parameters give rise to stress concentration within the material. When the porosity was low, the pores were away from each other, giving rise to isolated stress concentrations. At the higher porosity, these stress concentrations had interacting field, as the distance between the pores were reduced. At very high porosity levels, any small irregularities, like cracks, also interacted with the pores and raised the stress concentrations multifold. The above observation is in agreement with the conventionally processed porous materials [42]. Figure 12 also indicates that there was anisotropy in the mechanical properties of laser rapid manufactured porous structures. The value of yield stress is 226 MPa along the *X*- and *Y*-axes, while it is 254 MPa along the *Z*-axis for laser rapid manufactured samples of around 12% porosity. This difference in value is due to the LRM strategy. The reported tensile yield strength of the conventionally processed Inconel-625 is 414–758, 414–655 and 290–414 MPa in as rolled, annealed and solution annealed condition, respectively [23].

3.5 Microhardness measurement

The values of microhardness measurements were in the range of 256–370 $\mathrm{VHN}_{0.98\mathrm{N}}$ for laser rapid manufactured

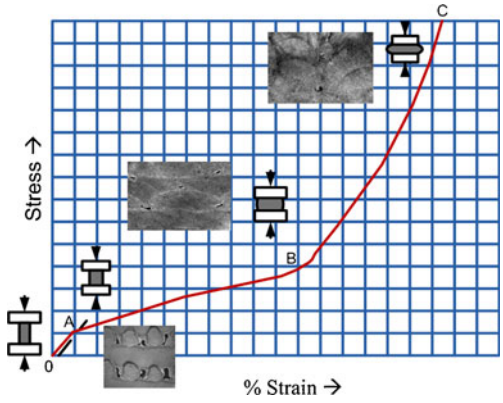

Fig. 11 Typical engineering stress–strain curve obtained during compressive strength testing of the laser rapid manufactured porous materials

porous materials. Table 7 presents the measured values of microhardness at different locations within track for samples, as shown in Fig. 13, processes at different processing parameters. It was seen that the microhardness value in the laser rapid manufactured sample did not depend on process parameters (like laser energy per unit traverse length, powder fed rate per unit traverse length) for the parametric range under investigation. It was because laser energy per unit traverse length within a certain range was needed for formation of continuous solid track for constant powder fed per unit transverse length. When laser energy per unit traverse length was reduced below a certain threshold, it resulted in discontinuous tracks. On the other hand, when it was increased above a certain value, it resulted in uneven porous tracks due to the excessive melting of feed material and flattening of track profile. When local variation of the microhardness within the track was studied, a higher value of microhardness was observed at the surface of the tracks near the pores. This was due to the rapid cooling and finer microstructure available at these locations. The observations were in agreement with earlier studies [26, 27].

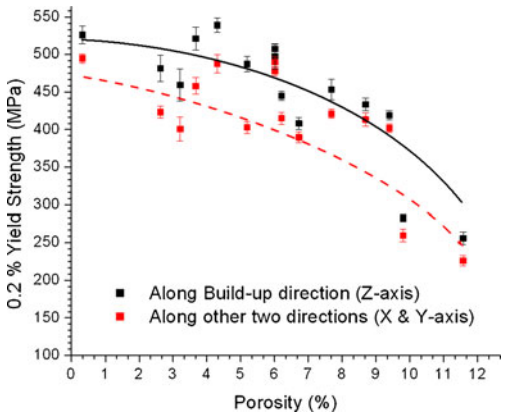

Fig. 12 The 0.2% yield strength as a function of the porosity for laser rapid manufactured porous materials

Table 7 Value of microhardness measurement of various porous samples

Sample ID	Side 1 (A)	Middle (B)	Side 2 (C)	Average
200901501	310	279	317	302.00
200901502	309	291	326	308.67
200901503	346.5	346.5	322	338.33
200901504	256	275	269	266.67
200901505	319	258	327	301.33
200901506	370	334	332	345.33
200901507	281	329	331	313.67
200901508	313	333	340	328.67
200901509	260	323	300	294.33
200901510	343	346	293	327.33
200901511	272	256	324	284.00
200901512	290	273	300	287.67
200901513	320	322	304	315.33
200901514	321	342	312	325.00
200901515	317	310	323	316.67

4 Conclusions

LRM of porous material using cross-thin-wall fabrication technique has been established, and a porosity of about 12% was achieved. The effect of various process parameters, such as laser power, scan speed, powder feed rate, transverse traverse index, number of layers, was studied. It was found that powder fed per unit traverse length, transverse traverse index and laser energy per unit traverse length affect the percentage porosity in descending order. A mathematical relation was developed to predict the percentage porosity with relevant processing parameters as input parameter using response surface methodology. This relation may be used to identify process parameters for functionally graded porosity. It was found that the laser rapid manufactured material had anisotropic mechanical properties due to LRM strategy. The compressive yield strength followed power law and decreased rapidly as the porosity was increased from 423±8 MPa for 2.63±0.14% porosity to 226±6.8 MPa for 11.57±0.52% porosity in

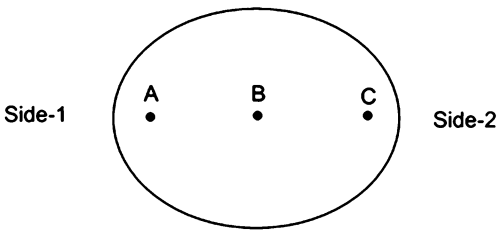

Fig. 13 Different locations used for microhardness measurement within track for porous LRM samples

fabricated porous material. The shape of the pores was triangular due to the cross thin walled fabrication strategy. There was variation in microhardness within the tracks due to fabrication strategy. The microhardness values were found to be in the range 256–370 $VHN_{0.98N}$. These studies are useful for the fabrication of porous structures with control on porosities and yield strengths for some of the potential prosthetic and engineering applications.

Acknowledgement The authors acknowledge the help of Dr. P. Ganesh for critical review of the manuscript. The technical support of the members of the Laser Materials Processing Division, RRCAT for carrying out experiments and characterizations is gratefully acknowledged.

References

1. Davis ME (2002) Ordered porous materials for emerging applications. Nature 417:813–821
2. Rubow KL (2009) Porous metal for aerospace. Adv Mater Process 167:26–28
3. Shapovalov V (1994) Porous metals. MRS Bull 19:24–28
4. Ryan G, Pandit A, Apatsidis DP (2006) Fabrication methods of porous metals for use in orthopaedic applications. Biomaterials 27:2651–2670
5. Ahsan MN, Paul CP, Kukreja LM, Pinkerton AJ (2011) Porous structures fabrication by continuous and pulsed laser metal deposition for biomedical applications: modelling and experimental investigation. J Mater Process Technol 211:602–609
6. Castilho M, Pires I, Gouveia B, Rodrigues J (2011) Structural evaluation of scaffolds prototypes produced by three-dimensional printing. Int J Adv Manuf Technol. doi:10.1007/s00170-011-3219-4
7. Laser Engineered Net Shaping (2002) http://www.sandia.gov/mst/pdf/LENS.pdf (accessed on May 30, 2011)
8. Xue L, Islam MU, Theriault A (2001) Laser consolidation process for the manufacturing of structural components for advanced robotic mechatronic system – a state of art review. In: Proceedings of 6th Int Symposium on Artificial Intelligence and Robotics & Automation in Space (i-SAIRAS 2001). Canadian Space Agency, Quebec, Canada, pp 1–8, AM080
9. Paul CP, Alemohammad H, Toyserkani E, Khajepour A, Corbin S (2007) Cladding of WC-12 Co on low carbon steel using a pulsed Nd:YAG laser. Mater Sci Eng, A 464:170–176
10. Davis SJ, Watkins KG, Dearden G, Fearon E, Zeng J (2006) Optimum deposition parameters for the direct laser fabrication (DLF) of quasi-hollow structures. In: Proc of Photon Conf. OPD, Manchester, pp 3–14
11. Song L, Singh VB, Dutta B, Mazumder J (2011) Control of melt pool temperature and deposition height during direct metal deposition process. Int J Adv Manuf Technol. doi:10.1007/s00170-011-3395-2
12. Moat RJ, Pinkerton A, Li L, Withers PJ, Preuss M (2009) Crystallographic texture and microstructure of pulsed diode laser-deposited Waspaloy. Acta Mater 5:1220–1229
13. Nowotny S, Scharek S, Beyer E, Richter K-H (2007) Laser beam build-up welding: precision in repair, surface cladding, and direct 3D metal deposition. J Therm Spray Tech 16:344–348
14. Imran MK, Masood SH, Brandt M (2010) Bimetallic dies with direct metal-deposited steel on Moldmax for high-pressure die casting application. Int J Adv Manuf Technol 52:855–863
15. Paul CP, Jain A, Ganesh P, Negi J, Nath AK (2006) Laser rapid manufacturing of Colmonoy-6 components. Opt Lasers Eng 44:1096–1109
16. Paul CP, Ganesh P, Mishra SK, Bhargava P, Negi J, Nath AK (2007) Investigating laser rapid manufacturing for Inconel-625 components. Opt Laser Technol 39:800–805
17. Ganesh P, Kaul R, Paul CP, Tiwari P, Rai SK, Prasad RC, Kukreja LM (2010) Fatigue and fracture toughness characteristics of laser rapid manufactured Inconel 625 structures. Mater Sci Eng, A 527:7490–7497
18. Santo L (2008) Laser cladding of metals: a review. Int J Surf Sci Eng 2:327–336
19. Toyserkani E, Khajepour A, Corbin S (2005) Laser cladding, 1st edn. CRC Press, Florida
20. Gu D, Shen Y (2008) Processing conditions and microstructural features of porous 316 L stainless steel components by DMLS. Appl Surf Sci 255:1880–1887
21. Li R, Shi Y, Wang Z, Wang L, Liu J, Jiang W (2010) Densification behavior of gas and water atomized 316 L stainless steel powder during selective laser melting. Appl Surf Sci 256:4350–4356
22. Li R, Liu J, Shi Y, Du M, Xie Z (2010) 316 L stainless steel with gradient porosity fabricated by selective laser melting. J Mater Eng Perform 19:666–671
23. Krishna BV, Bose S, Bandyopadhyay A (2007) Low stiffness porous Ti structures for load bearing implants. Acta Biomater 3:997–1006
24. http://www.specialmetals.com/documents/Inconel%20alloy%20625.pdf (accessed on May 30, 2011)
25. Thivillon L, Bertrand Ph, Laget B, Smurov I (2009) Potential of direct metal deposition technology for manufacturing thick functionally graded coatings and parts for reactors components. J Nucl Mater 385:236–241
26. Dinda GP, Dasgupta AK, Majumder J (2009) Laser aided direct metal deposition of Inconel 625 superalloy: microstructural evolution and thermal stability. Mater Sci Eng, A 509:98–104
27. Paul CP, Bhargava P, Ganesh P, Mishra SK, Premsingh CH, Kukreja LM (2008) Porous surface structures by continuous and pulsed laser direct metal deposition for biomedical applications. Proc Int Conf Process Fabri Adv Mater, New Delhi, India, pp 784–793
28. Nath AK, Reghu T, Paul CP, Ittoop MO, Bhargava P (2005) High-power transverse flow CW CO_2 laser for material processing applications. Opt Laser Technol 37:329–333
29. Paul CP, Bhargava P, Negi J, Nath AK (2003) Laser rapid manufacturing using Co-axial powder feeding system. In: Proc XIII National Conf Indian Soc Mech Engr. India, Roorkee, PE-071
30. Mumtaz KA, Erasenthiran P, Hopkinson N (2008) High density selective laser melting of Waspaloy®. J Mater Process Technol 195:77–87
31. How do you select an experimental design? (2010) http://www.itl.nist.gov/div898/handbook/pri/section3/pri33.htm#Response%20Surface%28method%29 (accessed on May 30, 2011)
32. Response surface methodology (2004) http://reports-archive.adm.cs.cmu.edu/anon/isri2004/CMU-ISRI-04-136.pdf (accessed on May 30, 2011)
33. ANOVA: ANalysis Of VAriance between groups (1996) http://www.physics.csbsju.edu/stats/anova.html (accessed on May 30, 2011)
34. ASTM Standard E9 (2009) Standard test methods of compression testing of metallic materials at room temperature. ASTM International, West Conshohocken, PA, 2003
35. ASTM Standard E384 (2009) E384-99e1 Standard test method for microindentation hardness of materials. ASTM International, West Conshohocken, PA

36. Lawrence J, Pou J, Low DK, Toyserkani E (eds) (2010) Advances in laser materials processing technology. Research and applications. CRC Press and Woodhead Publishing, Cambridge
37. Ahmed N, Voisey KT, McCartney DG (2010) Investigation into the effect of beam shape on melt pool characteristics using analytical modeling. Opt Lasers Eng 48:548–554
38. Peyre P, Aubry P, Fabbro R, Neveu R, Longuet A (2008) Analytical and numerical modelling of the direct metal deposition laser process. J Phys D Appl Phys 41:025403
39. Pinkerton AJ, Li L (2004) Modelling the geometry of a moving laser melt pool and deposition track via energy and mass balances. J Phys D Appl Phys 37:1885–1895
40. Pinkerton A, Wan W, Li L (2008) Component repair using laser direct metal deposition. Proc Inst Mech Eng B J Eng Manuf 222:827–836
41. Banhart J (2001) Manufacture, characterization and application of cellular metals and metal foams. Prog Mater Sci 46:559–632
42. Nakajima H (2007) Fabrication, properties and application of porous metals with directional pores. Prog Mater Sci 52:1091–1173